Acta Pharmacologica Sinica (2016) 37: 1259–1272
www.nature.com/aps

Open

Original Article

The structural basis of the dominant negative phenotype of the $G\alpha_{i1}\beta_1\gamma_2$ G203A/A326S heterotrimer

Ping LIU[1, #], Ming-zhu JIA[1, #], X Edward ZHOU[2], Parker W DE WAAL[2], Bradley M DICKSON[3], Bo LIU[1], Li HOU[1], Yan-ting YIN[1], Yan-yong KANG[2], Yi SHI[1], Karsten MELCHER[2], H Eric XU[1, 2, *], Yi JIANG[1, *]

[1]*VARI-SIMM Center, Center for Structure and Function of Drug Targets, CAS-Key Laboratory of Receptor Research, Shanghai Institute of Materia Medica, Chinese Academy of Sciences, Shanghai 201203, China;* [2]*Laboratory of Structural Sciences, Van Andel Research Institute, Grand Rapids, MI 49503, USA;* [3]*Center for Epigenetics, Van Andel Research Institute, Grand Rapids, MI 49503, USA*

Aim: Dominant negative mutant G proteins have provided critical insight into the mechanisms of G protein-coupled receptor (GPCR) signaling, but the mechanisms underlying the dominant negative characteristics are not completely understood. The aim of this study was to determine the structure of the dominant negative $G\alpha_{i1}\beta_1\gamma_2$ G203A/A326S complex (Gi-DN) and to reveal the structural basis of the mutation-induced phenotype of $G\alpha_{i1}\beta_1\gamma_2$.

Methods: The three subunits of the Gi-DN complex were co-expressed with a baculovirus expression system. The Gi-DN heterotrimer was purified, and the structure of its complex with GDP was determined through X-ray crystallography.

Results: The Gi-DN heterotrimer structure revealed a dual mechanism underlying the dominant negative characteristics. The mutations weakened the hydrogen bonding network between GDP/GTP and the binding pocket residues, and increased the interactions in the Gα-Gβγ interface. Concomitantly, the Gi-DN heterotrimer adopted a conformation, in which the C-terminus of $G\alpha_i$ and the N-termini of both the Gβ and Gγ subunits were more similar to the GPCR-bound state compared with the wild type complex. From these structural observations, two additional mutations (T48F and D272F) were designed that completely abolish the GDP binding of the Gi-DN heterotrimer.

Conclusion: Overall, the results suggest that the mutations impede guanine nucleotide binding and Gα-Gβγ protein dissociation and favor the formation of the G protein/GPCR complex, thus blocking signal propagation. In addition, the structure provides a rationale for the design of other mutations that cause dominant negative effects in the G protein, as exemplified by the T48F and D272F mutations.

Keywords: dominant negative; $G\alpha_{i1}\beta_1\gamma_2$ heterotrimer; G203A; A326S; crystal structure; GPCR; GDP

Acta Pharmacologica Sinica (2016) 37: 1259–1272; doi: 10.1038/aps.2016.69; published online 8 Aug 2016

Introduction

Guanine nucleotide-binding proteins, also named G proteins, play a vital role as molecular switches in signal transduction cascades initiated by the activation of G protein-coupled receptors (GPCRs). Inactive G proteins are heterotrimers that contain an α subunit and a βγ subunit. GDP occupies a binding pocket within the Gα subunit. GPCRs are activated by agonist binding, which induces conformational changes in the GPCRs that allow the association of their corresponding trimeric G proteins and promote the exchange of GDP to GTP within the Gα subunit. GTP binding causes conformational changes within the "switch" regions of the Gα subunit, thus leading to dissociation of the GTP-bound Gα subunit and the Gβγ dimer, which separately interact with downstream effectors. The slow intrinsic GTPase activity of the Gα subunit catalyzes the hydrolysis of GTP to GDP, thereby returning the Gα subunit to an inactivated state and resulting in re-association of the Gα and Gβγ subunits, which terminates the signal transduction.

Since the 1990s, high resolution crystal structures of the various stages of the G protein cycle in its active (GTPγS bound)[1–3], deactivated (GDP bound)[4, 5], inactive (Gαβγ complex)[6–8] and downstream effector-bound[9–11] states have been determined. In combination with extensive physiological and pharmacological studies, these structures shed light on the molecular basis for the function of heterotrimeric

# These authors contributed equally to this work.
*To whom correspondence should be addressed.
E-mail eric.xu@simm.ac.cn (H Eric XU);
yijiang@simm.ac.cn (Yi JIANG)
Received 2016-04-25 Accepted 2016-06-08

G proteins. The first structure of a GPCR-G protein complex, which was released in 2011, was a milestone[12] that provided a comprehensive structural basis for transmembrane signaling by GPCRs and G proteins. A recent breakthrough, the structure of the rhodopsin-arrestin complex, provides the basis for understanding the blocking of GPCR coupling to G proteins and arrestin-biased signaling[13]. These crystallographic studies have revealed three regions with major conformational differences between the GDP- and GTP-bound conformations of Gα, termed the switch I–III regions. Conformational changes in these regions are directly linked to the guanine nucleotide-binding domain, which is formed by five conserved loops called G1–G5 boxes (Figure 1). The G1–G3 boxes play a critical role in coordinating the α-, β-, and γ-phosphate groups and Mg^{2+}, whereas the G4–G5 boxes form the guanine ring-binding site.

Multiple steps in the G protein cycle can be interrupted by mutations in the Gα subunit, especially in the guanine nucleotide-binding pocket. These mutations cause the G protein cycle to be blocked, and the mutations have been used to delineate the GPCR-initiated signaling pathways. Several signaling-blocking mutations in the Gα subunit are dominant negative (DN) mutations, because they can block agonist-activated GPCR signaling in the presence of wild type G proteins. To date, there are three known mechanisms for DN mutation: the sequestration of the Gβγ subunits in a complex that is unable to bind activated GPCRs, the sequestration of the activated GPCR by a heterotrimeric complex that cannot exchange GDP and GTP, and the sequestration of the activated GPCR by nucleotide-free Gα[14].

Because GPCRs are targets for as many as 50% of drugs on the market, DN G proteins have been extensively used to delineate G protein signaling pathways and represent a promising tool to study GPCR-dependent signaling. A large

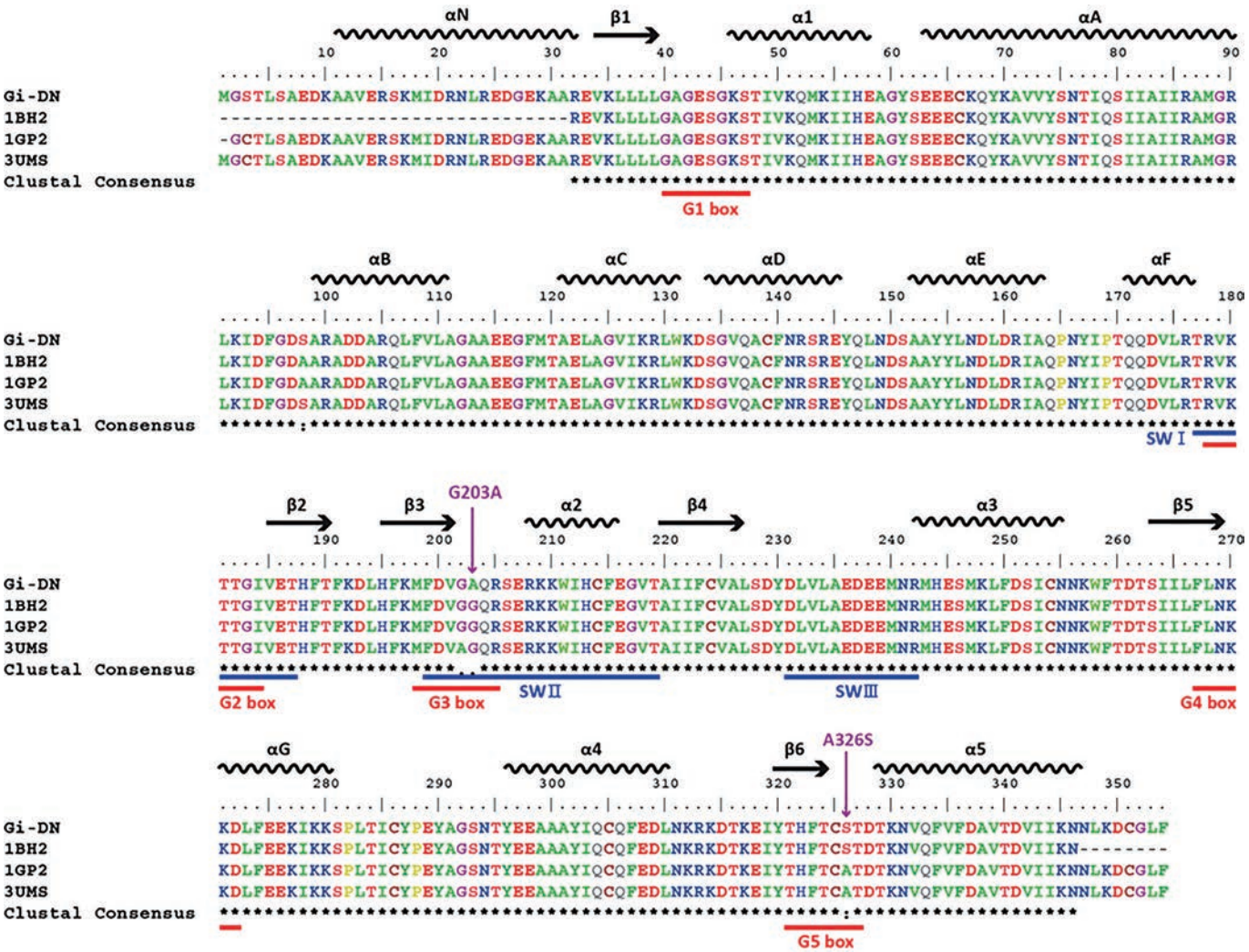

Figure 1. Sequence alignment of $G\alpha_i$-DN and homologous $G\alpha_i$. 1BH2, 1GP2, and 3UMS are PDB codes of already published $G\alpha_i$ structures. 1BH2, A326S mutant of $G\alpha_i$; 1GP2, wild type $G\alpha_i$; 3UMS, G202A mutant of $G\alpha_i$. Secondary structures are shown schematically above the sequences. The sequences of G1–G5 box are marked red, and the Switch I–III (SW I–III) are marked blue under the sequences. G203A and A326S mutations are highlighted by magenta arrows.

number of mutants with DN phenotypes have been identified for various types of G proteins: S54N in $G\alpha_s$[15], S47C in $G\alpha_o$[16], S48C in $G\alpha_{i2}$[17], G226A in $G\alpha_s$[18], G203T in $G\alpha_o$[19], D273N in $G\alpha_o$[20], and D277N in $G\alpha_{11}$[21]. Moreover, multiple DN Gα mutations have been combined to overcome conditional, nonselective, and weak mutant phenotypes[14]. For example, a triple Gα mutant, α3β5/G226A/A366S, almost completely inhibits Gα-mediated signaling[22], in which the α3β5 mutations replace five G residues in the α3 helix and the α3β5 loops with homologous $G\alpha_i$ residues (N271K, K274D, R280K, T284D, and I285T), which exhibit an enhanced affinity for GPCR. The G226A mutation stabilizes Gβγ binding, impairs the affinity of GTP, and prohibits the GTP-induced conformational change[23]. The A366S mutation decreases the affinity for GDP and GTPγS, probably by steric hindrance, and restrains Gαs in the empty nucleotide pocket state[24]. However, most DN phenotypes have been analyzed only functionally, whereas most structural studies have focused on Gα subunits with single mutations rather than G protein heterotrimers[8, 25, 26]. In contrast, the precise mechanisms of signal disruption in the context of G protein heterotrimers remain largely elusive. To gain further insight into the DN mechanism of the Gi heterotrimer, we constructed a multiple DN mutant, $G\alpha_i$ G203A/A326S, which corresponds to the G226A and A366S mutations in $G\alpha_s$, and determined its crystal structure.

Materials and methods

Expression and purification of the Gi-DN heterotrimer for crystallization

Construct design for *Spodoptera frugiperda* (Sf9) expression

The human $G\alpha_{i1}$, rat $G\beta_1$ and bovine $G\gamma_2$ open reading frames were codon-optimized and synthesized by using GENEWIZ (Suzhou, China). The C-terminus of $G\gamma_2$ was fused to the N-terminus of $G\alpha_{i1}$ containing G203A and A326S mutations by a 9 amino acid linker (GSAGSAGSA). The sequences encoding $G\beta_1$ and the $G\gamma_2$-$G\alpha_{i1}$ fusion protein were amplified using Phanta Super-Fidelity DNA Polymerase (Vazyme, Nanjing, China) and were separately subcloned into a modified pFastBac1 vector (Invitrogen, Cergy Pontoise, France), which contained an expression cassette for an 8×His tag and a codon-optimized maltose binding protein (MBP) tag followed by a Tobacco Etch Virus (TEV) protease recognition site upstream of the inserted fragments. In addition, single C to S point mutations were introduced at the C3 residue of $G\alpha_{i1}$ and the C68 residue of $G\gamma_2$, which are lipid modification sites, to abolish membrane targeting[27–29] and to allow for the purification of the G protein complex as soluble protein.

Virus generation and expression

High-titer recombinant baculovirus (>1×10^9 viral particles per mL) was obtained using the Bac-to-Bac Baculovirus Expression System (Invitrogen, Cergy Pontoise, France). Briefly, the pFastBac1 constructs were transformed into DH10Bac competent cells, and this was followed by standard blue/white α-complementation screening. Positive colonies were cultured and collected for bacmid extraction according to the standard protocol (Invitrogen, Carlsbad, CA, USA). The extracted bacmid DNAs were then transfected into Sf9 cells at a cell density of 1×10^6 cells/mL, and the Sf9 cell suspensions were cultured for 4 d at 27 °C with shaking at 300 r/min to generate the P1 generation virus. P1 and P2 viral stocks were amplified by infecting Sf9 cells at a cell density of 2×10^6–3×10^6 cells/mL, and they were isolated after 2 d. For the co-expression of the $G\gamma_2$-$G\alpha_{i1}$ and $G\beta_1$ subunits, Sf9 cells were co-transfected with two P2 viral stocks at a volume ratio of 1:3. The cells were collected after 36 h by centrifugation and stored at -80 °C until purification.

Purification of the Gi-DN heterotrimer

Frozen cell pellets were resuspended in a lysis buffer (pH 8.0) containing 20 mmol/L Tris, 200 mmol/L NaCl, 25 mmol/L imidazole, 10% glycerol and complete protease inhibitor cocktail (Roche, Basel, Switzerland). The cells were broken with a French Press with the pressure set at 1000 Pa. The lysate was centrifuged at 65000×*g* for 1 h, and the supernatant was loaded onto a nickel-chelating affinity column. After washing of the column with 30 column volumes of His Buffer A (20 mmol/L Tris, 200 mmol/L NaCl, 50 mmol/L imidazole, and 10% glycerol, pH 8.0), the protein was eluted with 5 column volumes of His Buffer B (20 mmol/L Tris, pH 8.0, 200 mmol/L NaCl, 300 mmol/L imidazole, and 10% glycerol). His-tagged TEV protease was then added to cleave the 8×His-MBP tag at the N-terminus of the $G\gamma_2$-$G\alpha_{i1}$ and $G\beta_1$ subunits. The sample was dialyzed against 20 mmol/L Tris, pH 8.0, 200 mmol/L NaCl, and 10% glycerol to remove the imidazole, and it was reloaded onto a nickel-chelating affinity column to remove the cleaved tag and non-cleaved protein. The untagged Gi-DN heterotrimer was collected in the flow-through of the column and concentrated to approximately 5 mg/mL using a 30 kDa MWCO spin filter (Millipore, Billerica, MA, USA). The concentrated protein was further purified through size exclusion chromatography with a HiLoad™ 16/600 Superdex™ 200 pg gel filtration column (GE Healthcare, Uppsala, Sweden) in size buffer (20 mmol/L Tris, pH 8.0, 200 mmol/L NaCl) at a flow rate of 0.5 mL/min with an AKTA FPLC (GE Healthcare, Pittsburgh, PA, USA). Fractions containing the monomeric Gi-DN heterotrimer were pooled, and the protein purity, homogeneity and stability were further assessed through SDS-PAGE, static light scattering and thermal stability analysis, respectively. The purified Gi-DN heterotrimer was concentrated to approximately 15 mg/mL for crystallization.

Crystallization, data collection and structure determination

Next, 200 μmol/L GDP was added to the purified protein prior to crystallization. Complex crystals were obtained with the sitting drop method in a buffer containing 2% *v/v* Tacsimate, pH 5.0; 0.1 mol/L sodium citrate tribasic dehydrate, pH 5.6; and 16% *w/v* PEG 3350. The crystals were transferred to a reservoir solution with 22% (*v/v*) ethylene glycol as a cryoprotectant before being flash frozen in liquid nitrogen. Data collection was performed at beamline BL17U1 of the Shanghai Synchrotron Radiation Facility (SSRF). To establish phase

information, the crystal structure of wild type $G\alpha_{i1}\beta_1\gamma_2$ heterotrimer (1GP2)[8] was used as the molecular replacement model. The structure was determined and refined with CCP4[30], Phenix[31], and COOT[32]. The data and refinement statistics are summarized in Table 1.

Table 1. Data collection and refinement statistics.

	Gi-DN heterotrimer
Data collection	
Space group	P21
Cell dimensions	
a, b, c (Å)	126.0, 54.6, 138.3
a, b, g (°)	90, 113, 90
Resolution (Å)	50–3.0 (3.15–3.00*)
Reflections	
Total/unique	220008/34720
R_{merge} (%)	22.9 (84.6*)
CC1/2	0.985 (0.766*)
I/sI	5.7 (1.9*)
Completeness (%)	98.4 (98.4*)
Redundancy	6.3 (5.4*)
Refinement	
Resolution (Å)	50–3.0
No reflections	34686
R_{work}/R_{free} (%)	27.6/30.5
No atoms in asu	
Protein	11499
Ligand/ion	56
Water	0
B-factors	
Wilson	46.8
Protein	96.7
Ligand/ion	34.5
Water	n.a.
r.m.s. deviations	
Bond lengths (Å)	0.003
Bond angles (°)	0.700
Ramachandran	
Favored (%)	98.0
Disallowed (%)	0.0
Molprobity score	1.3

* Values in parentheses are for highest-resolution shell.

Static light scattering

The average molecular mass of the Gi-DN heterotrimer was evaluated on a DAWN HELEOS-II instrument (Wyatt, Santa Barbara, CA, USA) connected in tandem to a high performance liquid chromatography system (Agilent, Santa Clara, CA, USA)[33]. A 20 μL sample at approximately 2 mg/mL was injected onto a Nanofilm SEC-250 (Sepax, Newark, DE, USA) column in size buffer (20 mmol/L Tris, pH 8.0, 200 mmol/L NaCl) at a flow rate of 0.35 mL/min. Because the light scattering intensity is directly proportional to the concentration and molecular weight, the molecular weight of the complex was calculated on the basis of the differential refractive index signals, which refers to concentration and the light scattering intensity.

Thermal shift assay (TSA)

The thermal stability of the $G\alpha_{i1}\beta_1\gamma_2$ heterotrimer was evaluated by using TSA as described previously[34]. Briefly, a mixture of 500 μg/L protein and 200 μmol/L GDP was incubated on ice for 30 min. Then, 5000× SYPRO Orange (Invitrogen, Carlsbad, CA, USA) was diluted with a size buffer and added to the reactions at a final concentration of ×5. All reactions were performed in triplicate in 384-well plates with a final volume of 10 μL. The thermal melting curve were monitored using a LightCycler 480 II Real-Time PCR System (Roche Diagnostics, Rotkreuz, Switzerland) with a ramp rate of 1 °C at the temperature range from 30 °C to 80 °C. The melting temperatures (T_m) were calculated by fitting the sigmoidal melting curve to the Boltzmann equation using GraphPad Prism with R^2 values of >0.99.

Molecular dynamic analysis

All-atom mollified adaptive biasing potential (mABP)[35]-biased simulations were performed using GROMACS5.0.5[36] in the canonical (NVT) ensemble with periodic boundary conditions and the CHARMM36-CAMP force field[37]. The GDP ligand parameters were generated with SwissParam[38] and combined with CHARMM36 parameters for ADP to obtain proper charges on the diphosphate group. The WT and DN GDP-bound $G\alpha_i$ monomers were prepared by removing the helical domain (ΔHD; residues 62–178[39]) using the crystallographic coordinates reported in this work. Each system was solvated in a 70×70×70 cube of TIP3P waters and 0.150 mmol/L NaCl (approximately 32500 atoms per system). Prior to the mABP simulations, 10 000 steps of energy minimization were followed by using 10 ns of isothermal–isobaric (NPT) equilibration with positional restraints on the protein backbone and GDP ligand. The pressure was maintained at 1 bar using the Berendsen barostat with a coupling time (t_p) of 1.0 ps and compressibility of 4.5×10^{-5} bar^{-1}. The temperature was maintained at 300 K using the v-rescale method with a coupling time of 0.1 ps. For production of mABP simulations in NVT, two tightly-coupled collective variables (CVs) were chosen to explore the interaction between WT and DN $G\alpha_i$ with GDP. The first CV is the RMSD of the GDP nucleotide head, and the second is the RMSD of the GDP phosphate groups, both with respect to their crystallographic positions. The CV space was discretized into a 480×480 bin grid with an RMSD range from 0 Å to 120 Å for a bin width of 0.25 Å. The mABP parameters were b=0.9 and c=0.001/Δt. A detailed discussion of these parameter selections has been addressed elsewhere[35]. Using mABP, both WTΔHD and DNΔHD were simulated for 1 μs in duplicate for a total of 4 μs.

Results

Purification and characterization of the Gi-DN heterotrimer

As described in the Methods, we co-expressed the subunits of the heterotrimer as a $G\gamma_2$-$G\alpha_{i1}$ fusion protein and a separate

$G\beta_1$ subunit by using a baculovirus system. Both proteins were expressed with an N-terminal tandem tag containing a 8×His tag, a codon-optimized MBP tag, and a TEV protease recognition site (Figure 2A). As shown in Figure 2B, most of the Gi-DN heterotrimer eluted as a monomer during size-exclusion chromatography. The SDS-PAGE analysis of the pooled eluate revealed two bands corresponding to molecular masses of 49 kDa and 38 kDa, which are the calculated masses of the $G\gamma_2$-$G\alpha_{i1}$ fusion protein and $G\beta_1$, respectively, with approximately 95% purity for the Gi-DN heterotrimer of (Figure 2B).

Static light scattering was used to evaluate the average molecular mass of the Gi-DN heterotrimer. The SEC elution profile, together with light scattering data and the differential refractive index signals, exhibited single peaks, thus indicating that the Gi-DN heterotrimer is highly homogeneous. A molecular mass of 90 kDa was determined by using multi-angle static light scattering, and this measurement was consistent with the calculated mass of the untagged Gi-DN heterotrimer (86.4 kDa) (Figure 2C).

We determined the stability of the Gi-DN heterotrimer by using a thermal shift assay. In the absence of exogenous GDP, the Gi-DN heterotrimer presented a lower T_m value (55.3 °C) than wild-type heterotrimer (61.1 °C), thus indicating that the decreased stability of the Gi heterotrimer was caused by G203A/A326S mutations. Additionally, in the presence of 200 μmol/L GDP, the T_m value of the Gi-DN heterotrimer increased from 55.3 °C to 60.0 °C, thus demonstrating that the Gi-DN heterotrimer was further stabilized by GDP (Figure 2D) and retained the capability to bind GDP.

Overall structure of the Gi-DN heterotrimer

The Gi-DN heterotrimer crystallized in space group $P2_1$, with two complexes in each asymmetric unit. Because the quality of the electron density maps for the first complex, which contains chain A, chain B and chain G, were better than that for the second one, which contains chain H, chain J and chain K, the following structural analysis of the Gi-DN heterotrimer was based on the first complex. A GDP molecule occupies the nucleotide-binding pocket formed by the interface between the $G\alpha_i$ Ras domain and the $G\alpha_i$ α-helical (AH) domain, and its presence stabilizes the interaction between these two domains (Figure 3A).

The conformation of the Gi-DN heterotrimer resembles that of the GDP-bound wild-type heterotrimer (PDB code 1GP2), with a root mean square deviation (RMSD) of 1.87 Å. Similarly to the wild-type Gi heterotrimer, the C-terminus of the Gγ subunit (E63-S68) and the N-terminus of the $G\alpha_{i1}$ subunits (M1-L5) could not be traced in the crystal structure of the Gi-DN heterotrimer. The 3×GSA linker between them also could not be traced, thus indicating that these flexible regions are less likely to affect the structure of the Gi-DN heterotrimer. Compared with the wild type structure, nearly all helices and loops in the $G\alpha_i$ subunit undergo movements accompanied

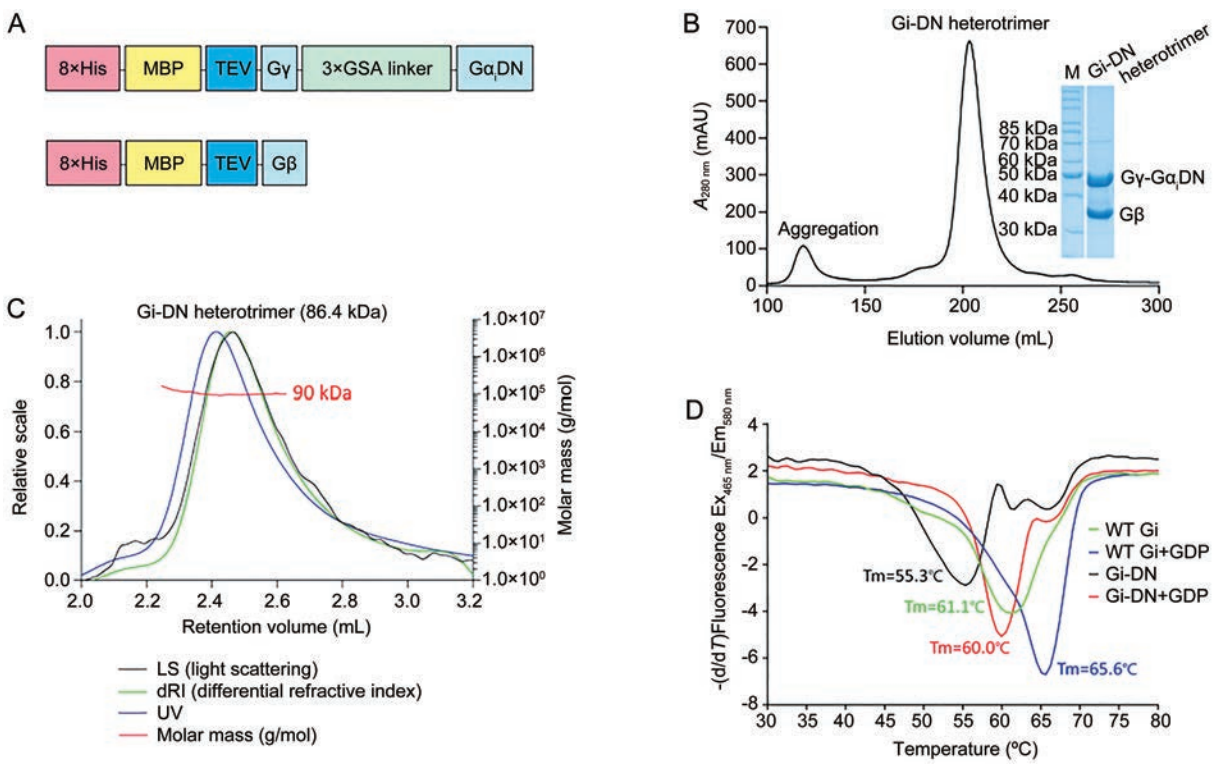

Figure 2. Expression, purification and characterization of Gi-DN heterotrimer. Schematic depiction of the expression constructs for Gγ-$G\alpha_i$ and Gβ. (B) A representative size-exclusion chromatography (SEC) elution profile for the Gi-DN heterotrimer. Pooled SEC elution fractions were analyzed by SDS-PAGE (B), Multi-Angle Static Light Scattering (C), and Thermal Shift Assay (D).

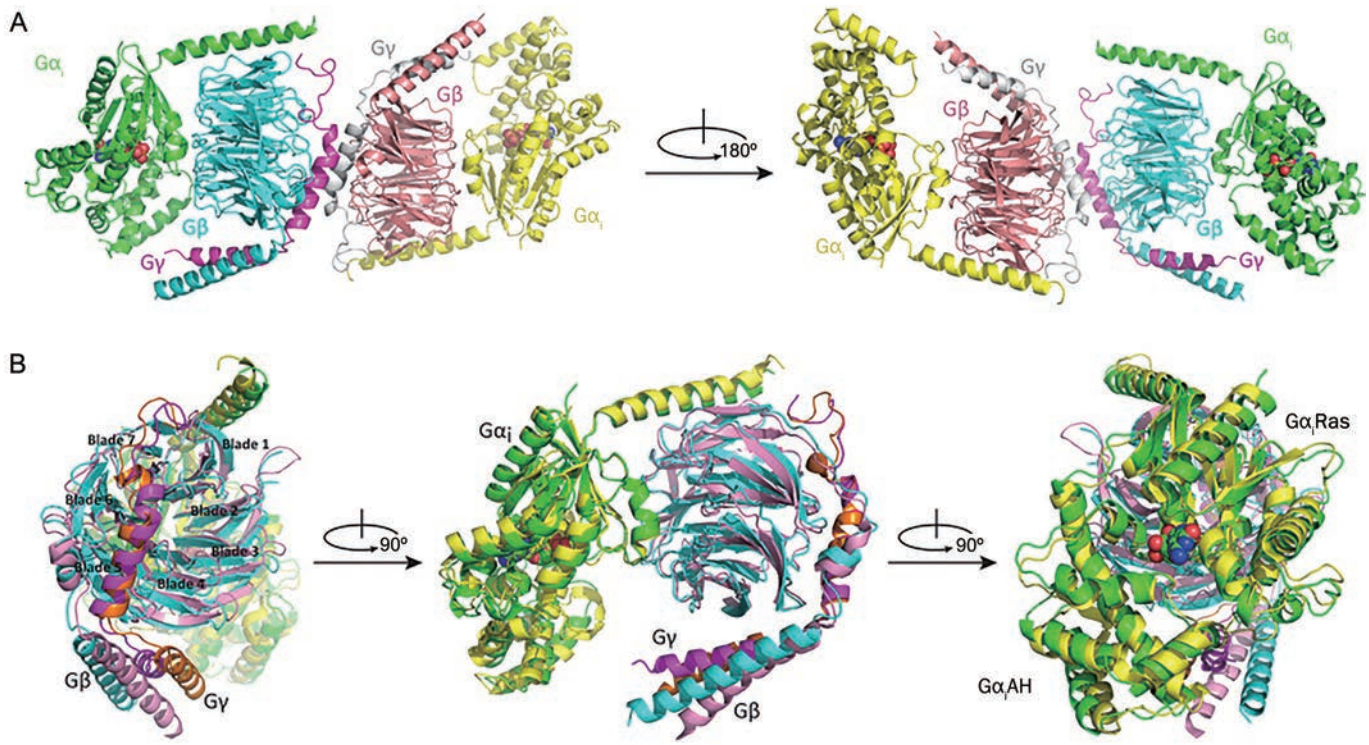

Figure 3. Overall structure of the Gi-DN heterotrimer and its comparison with GDP bound wild-type Gi heterotrimer (PDB code 1GP2). (A) The asymmetric unit contains two Gi-DN heterotrimers, one of which is composed of chain A ($G\alpha_i$, green), chain B (Gβ, cyan), chain G (Gγ, magenta), and the other one of chain H ($G\alpha_i$, yellow), chain J (Gβ, salmon), chain K (Gγ, gray). GDP is presented as spheres. (B) Comparison of Gi-DN and wild-type (PDB code 1GP2) heterotrimer structures in different views. The $G\alpha_i$, Gβ, and Gγ subunits of the Gi-DN heterotrimer are shown in green, cyan and magenta, and those of wild-type are shown in yellow, pink and orange, respectively. GDP is presented as spheres.

by the subtle displacement of the $G\alpha_i$AH domain away from $G\alpha_i$Ras domain. The β propeller, consisting of seven repeat blades of Gβ, also adopts a changed conformation through rotation, and this rotation is probably caused by the rearrangement of the $G\alpha_i$ subunit. Another notable structural difference between the Gi-DN and wild-type heterotrimer is the rotation and displacement of the parallel α-helical coiled coil formed by the amino terminus of the Gβ and Gγ subunits toward the $G\alpha_i$ subunit (Figure 3B).

Nucleotide-binding site

The structures of the $G\alpha_i$ subunits of the Gi-DN and wild-type heterotrimers were aligned to inspect differences in the guanine nucleotide-binding pocket, which is formed by five conserved loops, polypeptide boxes G1–G5. Distinct displacements were observed in the G2 and G3 boxes, which are responsible for the coordination of the γ-phosphate of GTP and mediate the major conformational changes upon activation by GTP. In addition, seven amino acids located in the switch III region were not resolved in the crystal structure, thus indicating their disorder in the DN mutant protein (Figure 4A).

We performed an analysis of the polar and hydrophobic interactions between GDP and the Gi-DN and wild-type heterotrimers by using the Ligplot+ program[40]. Although the extent of the Van der Waals interactions does not substantially differ, the hydrogen bonding network is rearranged. Compared with wild-type, the Gi-DN heterotrimer forms two extra hydrogen bonds between G1 box residues S47 and T44 and the α- and β-phosphates of GDP but loses four hydrogen bonds between the G4 box residues N269, K270, and D272 and the purine base of GDP (Figure 4B and 4C). The loss of two net hydrogen bonds indicates an attenuated GDP affinity for the Gi-DN heterotrimer. This speculation is supported by previous evidence that the A326S and G203A mutations in the $G\alpha_i$ subunit as well as the homologous mutations G226A and A366S in the $G\alpha_s$ subunit impair the affinity of the Gα subunit for GDP/GTPγS[23–26].

To understand why the A326S mutation attenuates GDP binding, we also performed mABP-biased MD simulations of the WTΔHD and DNΔHD GDP-bound $G\alpha_i$ monomer with the helical domain (ΔHD; herein referred to as WT and DN) removed[39]. Interestingly, significant changes in the conformational dynamics of the A326S-containing G5 box were observed between the WT and DN $G\alpha_i$. In contrast to the WT simulations, the introduction of a polar residue at A326S decreased the stability of the G5 box in both DN simulations and allowed it to move upward, 10 Å away from its crystallographic position (Figure 4D and 4E). From these simulations, it can be inferred that the A326S mutation destabilizes

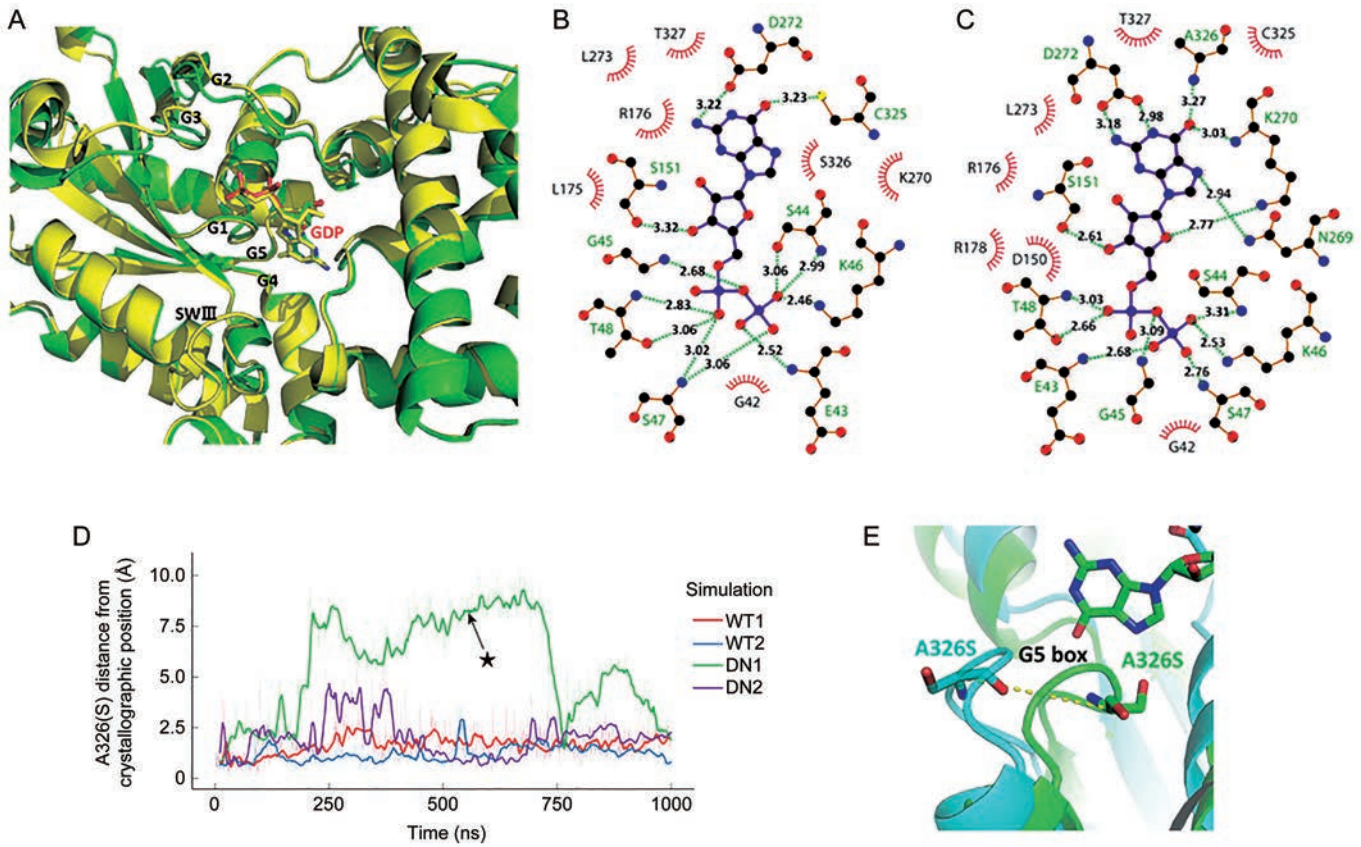

Figure 4. Nucleotide-binding site of GDP. (A) Alignment of $G\alpha_i$ in the Gi-DN and wild-type (PDB code 1GP2) Gi heterotrimers. $G\alpha_i$-DN is colored green and the wild-type protein in yellow. GDP is shown in stick presentation. (B, C) Ligplot+ interaction map of GDP and the binding pocket residues from Gi-DN (B) and wild-type Gi (PDB code 1GP2) (C). E43, S44, G45, K46, S47, and T48 are located in the G1 box, N269, K270, and D272 in the G4 box, C325, and A326 in the G5 box. (D and E) The A326S mutation destabilizes the G5 box. (D) Both DN simulations exhibit decreased stability of the G5 box with average displacements of 3.77±1.42 Å compared to 2.62 ± 0.58 Å for WT simulations. (E) Structural comparision between the crystal structure (green) and deformed G5 box (cyan; position in DN1 trajectory marked with asterisk in Figure 4D).

the binding pocket and thus may also contribute to the lower binding affinity for GDP and GTP.

G203, which is located in the G3 box loop, provides critical contacts for the γ-phosphate of GTP. To analyze the influence of the G203A mutation on GTP binding, we built a model of the GTP-bound form of Gi-DN based on the structure of the GTPγS-occupied $G\alpha_i$ A326S mutant protein (PDB code 1BH2)[25] by using SWISS-MODEL[41]. A steric clash between A203 and GTP was observed according to the alignment between the model and 1BH2 (Figure 5A), and the G3 box is rearranged, thus possibly reducing the steric conflict caused by the G203A mutation. In the DN-mutated structure, the backbone amide nitrogen atom of A203 is hydrogen-bonded to the backbone oxygen atom of T181 in the G2 loop, which contributes to the coordination of Mg^{2+} in the GTP-bound state. This hydrogen bond contact may cause the rearrangement, in which the G2 box moves toward the G3 box (Figure 5B).

A326 is located within 3.6 Å of the N7 atom of the guanine ring in the wild type Gi structure (PDB code 1GP2), and the A326S mutation is expected to cause a steric clash between the guanine ring and the slightly larger side chain of the A326S mutation. In the A326S mutant structure, the steric conflict between S326 and the purine base of GDP pushes GDP away from the S326 residue. The serine hydroxyl group is directed into the core of the Ras-like domain and forms a hydrogen bond with N269, thereby causing a conformational change in the residues in the G4 box. The shift of the guanine ring also distorts the perfect geometry of the hydrogen bonds between the carboxylate group of D272 and the two amine groups (N1 and N2) of the guanine base (Figure 5C). The combination of GDP displacement and the rearrangements of residues in the G4 box leads to the weakening of the binding of the A326S mutant to the guanine nucleotide (Figure 5D).

The interface of $G\alpha_i$ and Gβ

The $G\alpha_i$ and Gβγ subunits are assembled as a heterotrimer in the inactive state. The $G\alpha_i$ subunit is positioned at the narrow end of the channel formed by seven β blades of the Gβ subunit. The primary interaction between the $G\alpha_i$ and Gβ subunit comprises two interfaces, which are formed by the αN helix and switch II of the $G\alpha_i$ subunit and the β propeller of the Gβ

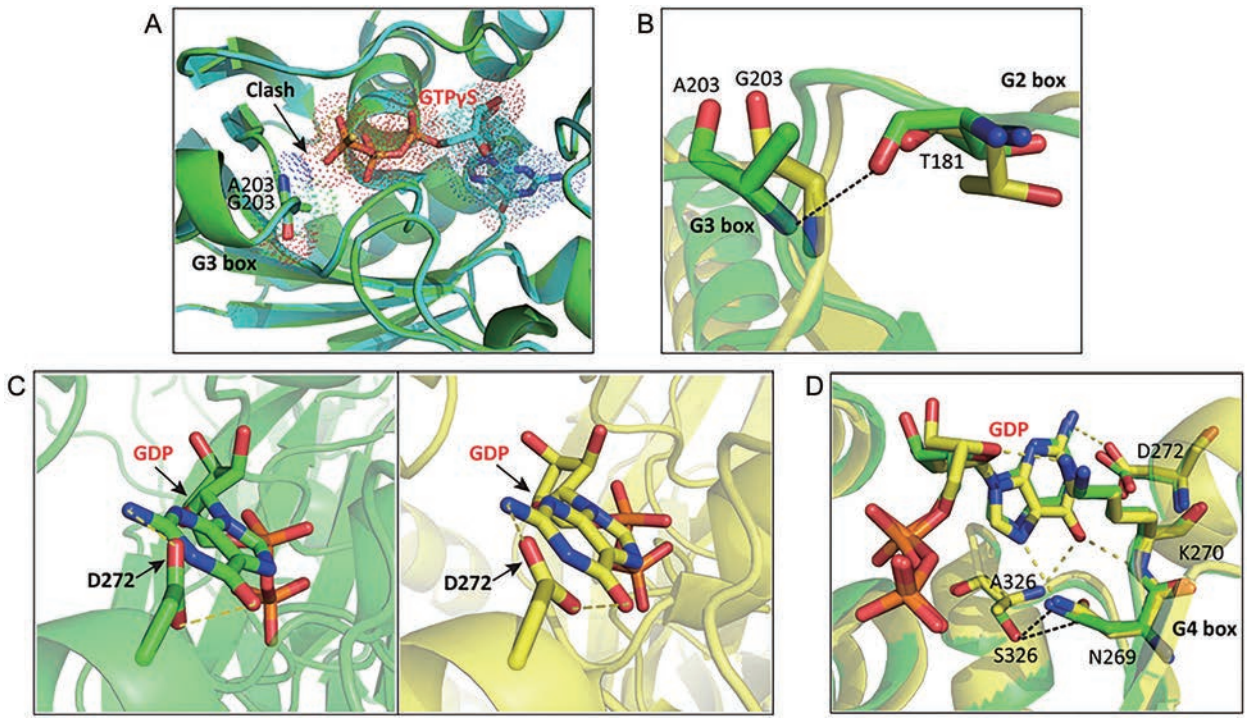

Figure 5. Effects of $G\alpha_i$ G203A and A326S mutations on guanine nucleotide binding. (A) Structural alignment of the GTPγS-bound A326S $G\alpha_{i1}$ (blue) (PDB code 1BH2) and the model of G203A mutation (green). The Van-der Waals spheres for G203A and GTP atoms are shown as dotted spheres, whose overlapping indicates space clash. (B) A203 forms a hydrogen bond with T181 located in the G2 box, resulting in a conformational change of the G2 box. (C) The geometry for the hydrogen bonds between the carboxylate group of D272 and the two amine groups (N1 and N2) of the guanine base. Left, Gi-DN heterotrimer; Right, wild type Gi heterotrimer (PDB code 1GP2). (D) The hydroxyl group of S326 introduces steric constraints for GDP, which causes S326 to move away from GDP. In addition, hydrogen bonds between S326 and N269 lead to conformational changes of their neighboring residues and is accompanied by loss of hydrogen bonds between GDP and N269, K270, and D272. In (B) and (D), the Gi-DN heterotrimer is shown in green and wild-type one is in yellow. The additional formed hydrogen bonds are shown as black dashed lines, and lost hydrogen bonds in Gi-DN heterotrimer are shown as yellow dashed lines.

subunit (Figure 6A). The total solvent-accessible surface area (SASA) buried in the $G\alpha_i$-Gβ interface caculated by PISA in the CCP4 suite is 1193.4 $Å^2$ in the Gi-DN heterotrimer compared with 1145.3 $Å^2$ in the wild type heterotrimer, thus indicating more extensive Gα-Gβ contacts in the Gi-DN heterotrimer.

The amino-terminal helix of $G\alpha_i$ packs across the D strands of blade 1 and blade 7 of Gβ. In the Gi-DN structure, the αN helix of the $G\alpha_i$ subunit undergoes a rotation and displacement away from blade 7 and toward blade 1 (Figure 6D), thus resulting in the loss of an ionic interaction between the oxygen atom of the D20 side chain in the $G\alpha_i$ subunit and the guanidyl group of R52, which is located in the D strand of blade 7 of the Gβ subunit. This displacement also creates two extra hydrogen bonds between the αN helix of $G\alpha_i$ subunit and the D strand of blade 1 of the Gβ subunit; the R15 guanidyl group is hydrogen bonded to the backbone oxygen atom of V90 and the ND1 atom in the imidazole ring of H91 (Figure 6B and 6C, Table 2).

Interface 2 mainly consists of switch II, which is also critical for the binding of the γ-phosphate of GTP and the coordination of Mg^{2+}. Thus, the exchange of GDP for GTP or the hydrolysis of GTP is closely associated with the affinity of the interaction between the $G\alpha_i$ and Gβγ subunits. The switch II displacement of the Gi-DN heterotrimer differs from that of wild type for nearly every residue in switch II. Additionally, the β propeller loops at the $G\alpha_i$-Gβ interface also adopt a changed conformation. The resultant conformational changes in $G\alpha_i$ and Gβ lead to distinct contacts in interface 2 (Figure 6E–6G). For example, N119 in Gβ extends toward the $G\alpha_i$ subunit and forms two additional hydrogen bonds with the backbone oxygen atom and the hydroxyl oxygen of T182 in switch I, while the hydrogen bond between E186 in the $G\alpha_i$ subunit and W99 in the Gβ subunit is broken by a 1 Å outward movement of the β2 strand (Figure 6E and 6F, Table 2).

A complete comparison of the interactions in the $G\alpha_i$-Gβ interface shows that the Gi-DN heterotrimer has three more pairs of polar contacts than the wild type complex (Table 2), consistently with the increased size of the buried interface, suggesting increased stability of Gα-Gβ interaction in the Gi-DN heterotrimer. The more extensive interactions at the Gα-Gβγ interface have been supported by previous reports. The G203A mutation in $G\alpha_i$ and the homologous G226A mutation in $G\alpha_s$ inhibit the conformational changes that occur after GTP binding and consequently inhibit the release of Gβγ subunits[18, 26].

Table 2. Polar interactions on the $G\alpha_i$ and Gβ interface.

	Atom in $G\alpha_i$	Atom in Gβ	Distance (Å)*	
αN	R15 NH1	V90 O	2.2	Interface 1
	R15 NH2	H91 ND1	3.3	
	S16 OG	K89 N	2.9 / 3.1	
	D20 OD1	K89 NZ	3.2 / 3.0	
	D20 OD1	R52 NH1	3.0	
	D26 OD1	K78 NZ	2.8 / 3.6	
G2 box	T182 O	N119 ND2	2.9	Interface 2
	T182 OG1	N119 ND2	3.5	
	I184 N	L117 O	3.3 / 2.9	
β2	E186 OE1	W99 NE1	3.1	
β3-α2 Loop	Q204 OE1	Y145 N	2.6 / 3.2	
	Q204 NE2	L117 O	3.3 / 3.2	
	Q204 NE2	N119 OD1	3.1 / 3.0	
	R205 N	T143 O	3.3	
	E207 N	D186 OD1	2.9 / 3.1	
α2	K209 NZ	D246 OD1	3.1	
	K210 NZ	D228 OD1	3.5 / 2.9	
	K210 NZ	D246 OD1	3.1 / 3.3	
	K210 NZ	N230 OD1	3.1	
	K211 NZ	N230 OD1	3.1	
	H213 O	K57 NZ	3.3	
	H213 ND1	Y59 OH	3.5	
	C214 O	Q75 NE2	3.5	
	E216 OE1	K57 NZ	3.3 / 2.8	

* The distance data for Gi-DN heterotrimer are shown as red, and that for wild type Gi (PDB code 1GP2) are shown as blue.

The Gi-DN heterotrimer adopts structural features of the G protein in the receptor-bound state

The most surprising observation in the Gi-DN heterotrimer structure is the large displacement of the α-helical N-termini of Gβ and Gγ toward the $G\alpha_i$ subunit relative to wild type complex (Figure 7A), which closely resembles the conformations of the N-termini in the β_2AR-$G\alpha_s\beta\gamma$ complex (3SN6) (Figure 7B). Two additional hydrogen bonds in the Gi-DN heterotrimer are likely to be responsible for this displacement. The hydroxyl group of Gβ T221 forms a hydrogen bond with the carbonyl group of Gγ E22, and the side chain amide nitrogen of Q259 hydrogen bonds with the backbone oxygen of Gβ R22, thus stabilizing the proximally located the $G\alpha_i$ subunit and the N-termini of the Gβ or Gγ subunits, respectively (Figure 7C and 7D). The same two hydrogen bonds also contribute to the shift in the Gβ and Gγ N-termini in the β_2AR-$G\alpha_s\beta\gamma$ complex (not shown).

The penetration of the C-terminal α5 helix of the G protein into the cytoplasmic core of the transmembrane bundle of the activated GPCRs is one of the most striking structural features of the GPCR-G protein interaction. The substitution of A326 with S alters the conformation of the β6-α5 loop, leading to a distinct shift in the α5 helix of the Gα subunit in the Gi-DN heterotrimer, although this shift is smaller in magnitude compared with the one in the receptor-bound state of $G\alpha_s\beta\gamma$ in the structure of the β_2AR-$G\alpha_s\beta\gamma$ complex (Figure 7E). Overall, we conclude that the Gi-DN heterotrimer shares features of the G protein in a receptor-bound state.

The effects of extra mutations in the GDP-binding pocket on the thermal stability of the Gi-DN heterotrimer

Although GDP is still observed in our structure of the Gi-DN heterotrimer, a more potent DN mutant may be expected to completely block GDP binding. To test this possibility, we introduced four extra single point mutations that alter residues in the GDP-binding pocket (D150L, C325I, T48F, and D272F) based on our Gi-DN structure. We purified the corresponding mutant proteins and tested their thermal stability in the presence or absence of GDP (Figure 8A). The thermal stability curves of the D150L and C325I mutants notably shifted to increased T_m values in the presence of 200 μmol/L GDP, indicating that D150 and C325 are not required for GDP binding (Figure 8B–8D). In contrast, the mutations T48F and D272F in the Gi-DN heterotrimer exhibited similar T_m values in both the presence and absence of GDP (Figure 8E and 8F), implying that both T48F and the D272F mutations can prevent GDP binding. The T_m values of these two mutant proteins were approximately 50 °C lower than that of the DN mutant control (60 °C in the presence of GDP), in accordance with the previously reported reduced stability of the guanine nucleotide free G protein[23].

To reveal the molecular mechanism by which T48F and D272F block GDP binding, we built two mutant protein homology models based on the structure of human $G\alpha_{i1}$ G202A (PDB code 3UMS)[42]. The benzene ring of F48 in the model sterically interferes with the position of the ribose ring (Figure 8G), and F272 almost overlaps with the guanine base, which would prevent GDP access to the pocket (Figure 8H) and further destabilize the Gi-DN heterotrimer.

Discussion

Several dominant negative Gα subunits have been developed to investigate GPCR-G protein signaling pathways. Despite the progress that has been made in understanding the DN effects of G proteins in terms of functional evaluations, the molecular mechanisms of GPCR-dependent signal disruption by DN mutants remains elusive because of the scarcity of the structural evidence for G protein heterotrimers. Here, we solved the structure of G203A and A326S mutated $G\alpha_{i1}\beta_1\gamma_2$, and we provide the first report of the DN mechanism caused by these mutations.

By comparing the structure of the wild type Gi heterotrimer, we observed subtle conformation changes in the nucleotide-binding pocket that attenuate the affinity for GDP, more extensive contacts in the interface between the Gα subunit and Gβγ-dimer, a distinct displacement of the N-terminal helices of both Gβ and Gγ subunits and a stretch upward of the αC helix in the Gα subunit. In addition, molecular dynamic analysis indicated that the nucleotide-binding pocket of Gα is

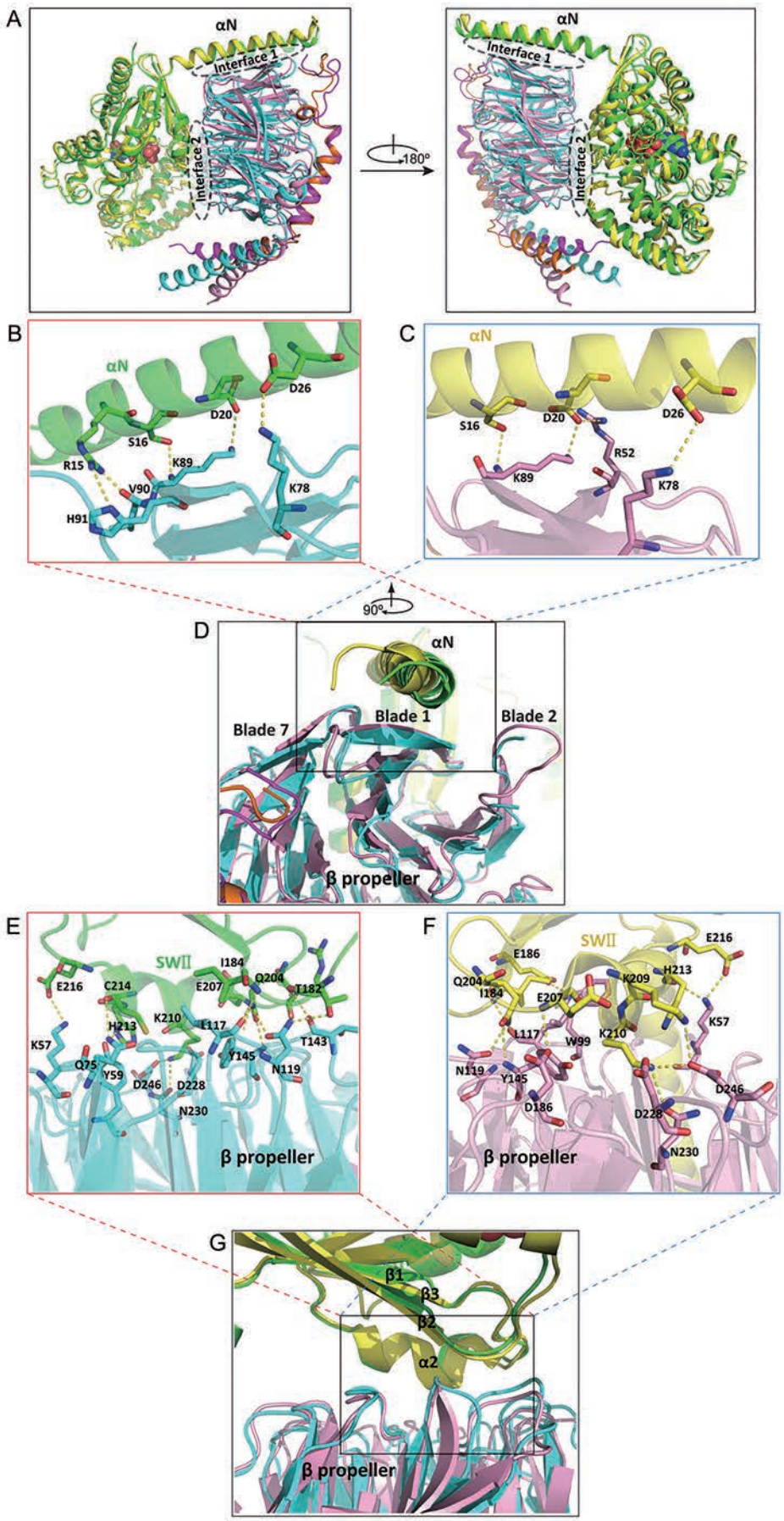

Figure 6. The interface and polar contacts between $G\alpha_i$ and Gβ subunits. (A) The two interfaces between $G\alpha_i$ and Gβ subunits of the Gi-DN and wild-type (PDB code 1GP2) heterotrimers. The α subunits of DN-Gi and wild type Gi are colored in green and yellow, and the β subunits in blue and pink, respectively. (B–D) Polar contacts in interface 1 of DN-$G\alpha_i$ and Gβ are rotated and displaced from blade 7 towards blade 1 (D). The number of polar contacts in Gi-DN (B) is five and in the wild-type complex (C) four. (E–G) Polar contacts in interface 2 of the $G\alpha_i$ and Gβ subunits (G). The number of polar contacts in Gi-DN (E) is fourteen and in wild-type (F) is twelve.

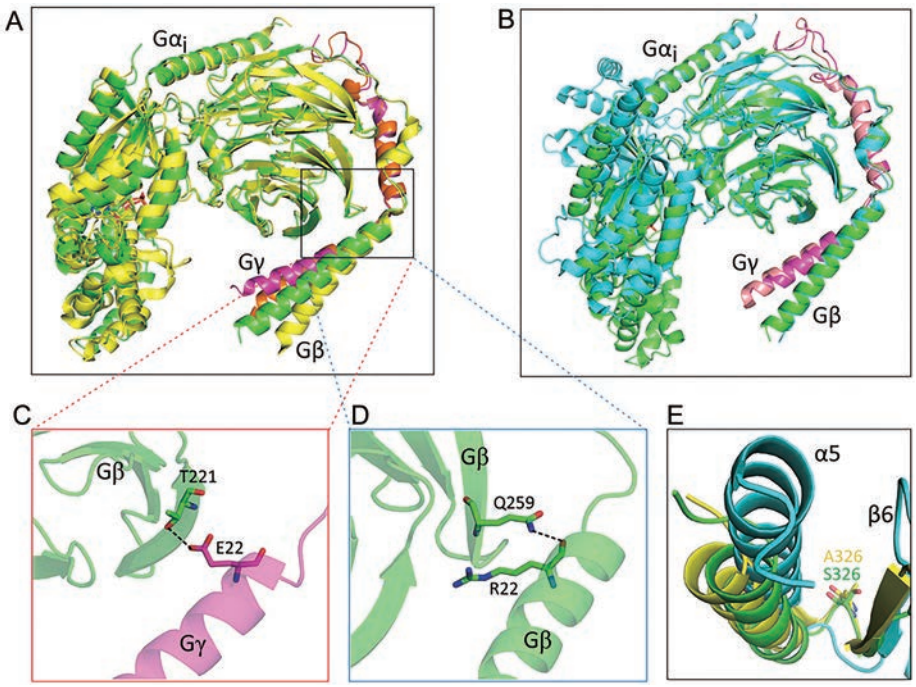

Figure 7. The Gi-DN heterotrimer shares conformational features with G protein in the receptor-bound state. (A) Structure alignment of the Gi-DN and wild type heterotrimers (PDB code 1GP2). The Gi-DN Gα and Gβ subunits are shown in green and the Gγ subunit in light magenta. For the wild-type Gi heterotrimer, Gα and Gβ are shown in yellow and Gγ in orange. (B) Alignment of Gi-DN heterotrimer with the $G\alpha_s\beta\gamma$ trimer in the β_2AR-bound state (PDB code 3SN6), with Gα and Gβ shown in blue and Gγ in salmon. The subunits of the Gi-DN heterotrimer are shown with same colors as in (A). (C) Hydrogen bond between T221 in Gβ and E22 in Gγ. The Gβ subunit is shown in green and Gγ in light magenta. (D) Hydrogen bond between Q259 and R22 in the Gβ subunit. (E) Superposition of the α5 helices from the Gi-DN heterotrimer (green), wild type heterotrimer (yellow) and the heterotrimer from the β_2AR-$G\alpha_s\beta\gamma$ complex (blue).

greatly destabilized by G203A/A326S mutations, thus potentially contributing to its lower binding affinity for GDP and GTP. We speculate that the Gi-DN heterotrimer is characterized by a reduced affinity for both GDP and GTP, leading to a preference for a nucleotide-free state. Thus, the Gi-DN protein fails to accomplish the exchange of GDP for GTP and loses the ability to be activated. The enhanced interaction of the Gα subunit with Gβγ also prevents the dissociation of Gβγ from the heterotrimer, thereby preventing downstream effector activation by the separate subunits. Surprisingly, the Gi-DN heterotrimer adopts the structural features of the G protein in the receptor-bound state, indicating that Gi-DN is in a state that interacts more easily with activated GPCR than wild type G proteins.

The Gi-DN heterotrimer attenuates the binding of activated GPCRs with endogenous wild type G proteins in two different ways. First, it sequesters Gβγ with a relatively more potent binding capability, consequently preventing the wild-type Gα from binding to Gβγ, a process indispensable for binding to the activated GPCR. In addition, the Gi-DN heterotrimer preferentially occupies an activated GPCR, thus decreasing the possibility of the stimulation of other wild type G proteins by GPCR and blocking the physiological transducing signal of GPCR.

We also found that two extra mutations in the GDP binding pocket have the potential to abolish GDP binding by the Gi-DN heterotrimer. The Gi-DN heterotrimer with mutations T48F and D272F, together with G203A/A326S, did not display a thermal shift after incubation with GDP, thus that these two mutations are likely to abolish GDP binding completely and to lead to a nucleotide-free state of the Gi heterotrimer. This result is consistent with the rationale for the T48F and D272F mutations, which is that the large side chains of the mutated phenyalanine interfere with the binding of the $G\alpha_i$ subunit to the guanine ring.

Dominant negative G proteins are frequently used to delineate GPCR-mediated signaling pathways and to exhibit potential usefulness in therapeutic applications[43]. The dominant negative mechanism revealed in this study provides a solid structural basis for the design of more potent mutants. However, the structural study of the GPCR-G protein complex is crucial to the research of overall GPCR signal pathways; however, the GPCR-G protein complex is difficult to crystallize because of its considerable instability when binding to GDP or GTP. In the structural study of the β_2AR-Gs complex, GDP was removed from its binding pocket by apyrase[12] to diminish the influence of GDP. As we characterized previously, the DN-Gi mutant appears to stabilize the Gαβγ-receptor complex with a reduced nucleotide affinity. Dominant negative G proteins are expected to favor the stability of the GPCR-G protein

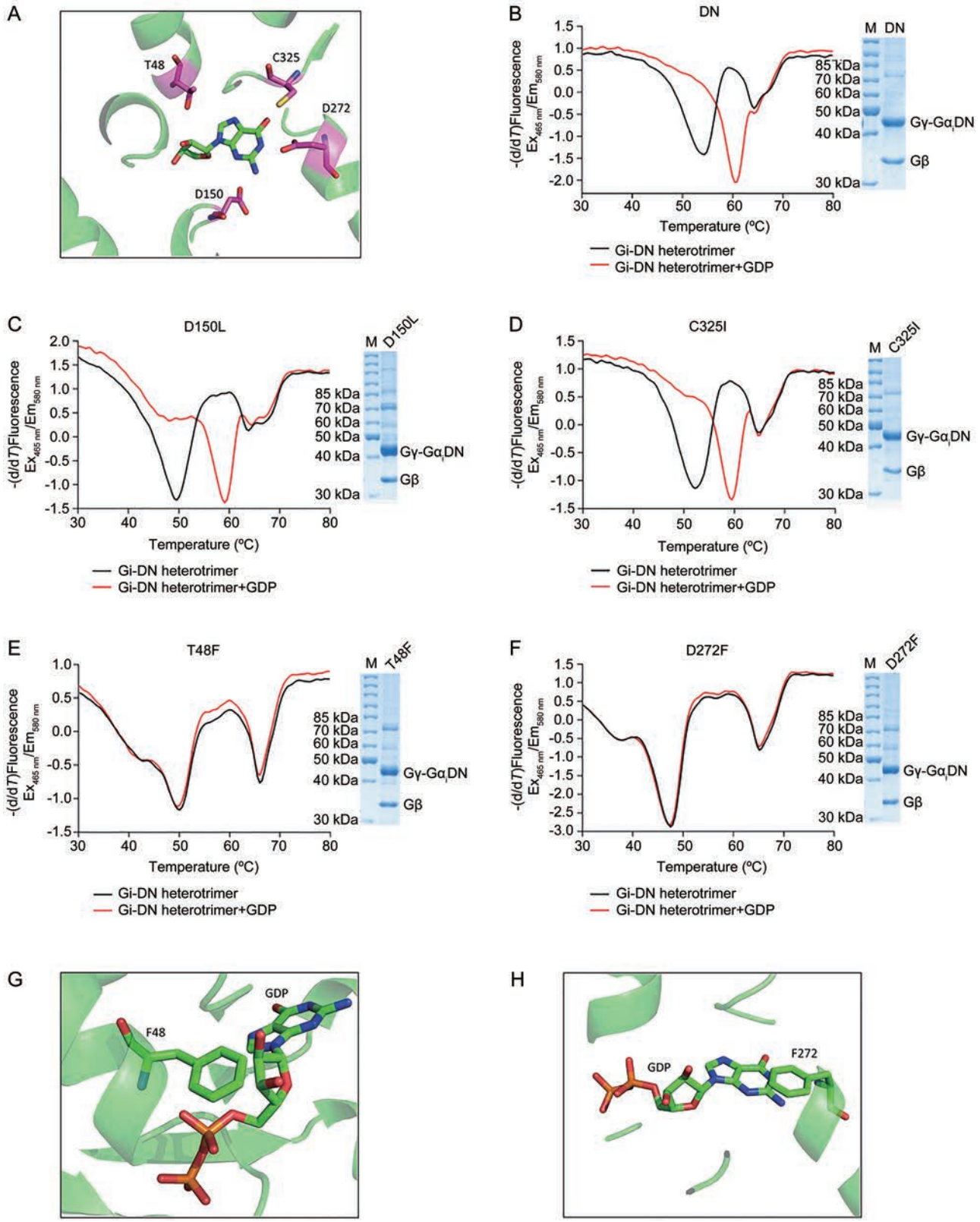

Figure 8. Effects of additional mutations introduced into the GDP binding pocket on thermal stability of the Gi-DN heterotrimer. (A) GDP in the $G\alpha_i$-DN binding pocket. Pocket residues selected for mutagenesis are shown in stick presentation. (B–F) Thermal shift and corresponding SDS-PAGE profiles of mutant Gi-DN heterotrimers. Negative control (Gi-DN without additional mutations; B), Gi-DN D150L (C), Gi-DN C325I (D), Gi-DN T48F (E), and Gi-DN D272F (F). A GDP-induced thermos-shift was observed for Gi-DN, D150L, and C325I but not for T48F and D272F mutants. (G) Structure modeling of the T48F mutation. (H) Structure modeling of the D272F mutation.

complex and to provide an alternative means for the structural study of the GPCR-G protein complex.

Acknowledgements

This work was supported by grants from the National Natural Science Foundation of China (31300607); the Shanghai Science and Technology Committee (13ZR1447600); the Shanghai Rising-Star Program (14QA1404300); the Outstanding Young Scientist Foundation, Chinese Academy of Sciences (CAS); the Youth Innovation Promotion Association CAS; the SANOFI-SIBS Scholarship; in part by the Jay and Betty Van Andel Foundation, Amway (China); and the Ministry of Science and Technology of China (No 2012CB910403, 2013CB910601, and XDB08020303).

Author contribution

Ping LIU and Ming-Zhu JIA designed and performed the research and wrote the first draft of the paper. Edward ZHOU solved and analyzed the structure. Parker W DE WAAL and Bradley M DICKSON analyzed the structure and the molecular dynamic analysis. Bo LIU, Li HOU, Yan-ting YIN, and Yan-yong KANG performed the research. Yi SHI and Karsten MELCHER revised and commented on the manuscript. H Eric XU and Yi JIANG supervised the project and wrote the manuscript with contributions from all the authors.

References

1 Sunahara RK, Tesmer JJ, Gilman AG, Sprang SR. Crystal structure of the adenylyl cyclase activator Gsalpha. Science 1997; 278: 1943–7.
2 Coleman DE, Berghuis AM, Lee E, Linder ME, Gilman AG, Sprang SR. Structures of active conformations of Gi alpha 1 and the mechanism of GTP hydrolysis. Science 1994; 265: 1405–12.
3 Noel JP, Hamm HE, Sigler PB. The 2.2 A crystal structure of transducin-alpha complexed with GTP gamma S. Nature 1993; 366: 654–63.
4 Mixon MB, Lee E, Coleman DE, Berghuis AM, Gilman AG, Sprang SR. Tertiary and quaternary structural changes in Gi alpha 1 induced by GTP hydrolysis. Science 1995; 270: 954–60.
5 Kreutz B, Yau DM, Nance MR, Tanabe S, Tesmer JJ, Kozasa T. A new approach to producing functional G alpha subunits yields the activated and deactivated structures of G alpha(12/13) proteins. Biochemistry 2006; 45: 167–74.
6 Lambright DG, Sondek J, Bohm A, Skiba NP, Hamm HE, Sigler PB. The 2.0 A crystal structure of a heterotrimeric G protein. Nature 1996; 379: 311–9.
7 Nishimura A, Kitano K, Takasaki J, Taniguchi M, Mizuno N, Tago K, *et al.* Structural basis for the specific inhibition of heterotrimeric Gq protein by a small molecule. Proc Natl Acad Sci U S A 2010; 107: 13666–71.
8 Wall MA, Coleman DE, Lee E, Iniguez-Lluhi JA, Posner BA, Gilman AG, *et al.* The structure of the G protein heterotrimer Gi alpha 1 beta 1 gamma 2. Cell 1995; 83: 1047–58.
9 Kimple RJ, Kimple ME, Betts L, Sondek J, Siderovski DP. Structural determinants for GoLoco-induced inhibition of nucleotide release by Galpha subunits. Nature 2002; 416: 878–81.
10 Tesmer JJ, Sunahara RK, Gilman AG, Sprang SR. Crystal structure of the catalytic domains of adenylyl cyclase in a complex with Gsalpha. GTPgammaS. Science 1997; 278: 1907–16.
11 Slep KC, Kercher MA, He W, Cowan CW, Wensel TG, Sigler PB. Structural determinants for regulation of phosphodiesterase by a G protein at 2.0 A. Nature 2001; 409: 1071–7.
12 Rasmussen SG, DeVree BT, Zou Y, Kruse AC, Chung KY, Kobilka TS, *et al.* Crystal structure of the beta2 adrenergic receptor-Gs protein complex. Nature 2011; 477: 549–55.
13 Kang Y, Zhou XE, Gao X, He Y, Liu W, Ishchenko A, *et al.* Crystal structure of rhodopsin bound to arrestin by femtosecond X-ray laser. Nature 2015; 523: 561–7.
14 Barren B, Artemyev NO. Mechanisms of dominant negative G-protein alpha subunits. J Neurosci Res 2007; 85: 3505–14.
15 Hildebrandt JD, Day R, Farnsworth CL, Feig LA. A mutation in the putative Mg(2+)-binding site of Gs alpha prevents its activation by receptors. Mol Cell Biol 1991; 11: 4830–8.
16 Slepak VZ, Quick MW, Aragay AM, Davidson N, Lester HA, Simon MI. Random mutagenesis of G protein alpha subunit G(o)alpha. Mutations altering nucleotide binding. J Biol Chem 1993; 268: 21889–94.
17 Slepak VZ, Katz A, Simon MI. Functional analysis of a dominant negative mutant of G alpha i2. J Biol Chem 1995; 270: 4037–41.
18 Lee E, Taussig R, Gilman AG. The G226A mutant of Gs alpha highlights the requirement for dissociation of G protein subunits. J Biol Chem 1992; 267: 1212–8.
19 Van-Ham II, Lupu-Meiri M, Tayer M, Shapira H, Oron Y. Response to lysophosphatidic acid in *Xenopus* oocytes and its rapid desensitization: the role of Gq and Go G-protein families. J Cell Physiol 2004; 200: 125–33.
20 Yu B, Slepak VZ, Simon MI. Characterization of a Goalpha mutant that binds xanthine nucleotides. J Biol Chem 1997; 272: 18015–9.
21 Yu B, Gu L, Simon MI. Inhibition of subsets of G protein-coupled receptors by empty mutants of G protein alpha subunits in g(o), G(11), and G(16). J Biol Chem 2000; 275: 71–6.
22 Berlot CH. A highly effective dominant negative alpha s construct containing mutations that affect distinct functions inhibits multiple Gs-coupled receptor signaling pathways. J Biol Chem 2002; 277: 21080–5.
23 Iiri T, Bell SM, Baranski TJ, Fujita T, Bourne HR. A Gsalpha mutant designed to inhibit receptor signaling through Gs. Proc Natl Acad Sci U S A 1999; 96: 499–504.
24 Iiri T, Herzmark P, Nakamoto JM, van Dop C, Bourne HR. Rapid GDP release from Gs alpha in patients with gain and loss of endocrine function. Nature 1994; 371: 164–8.
25 Posner BA, Mixon MB, Wall MA, Sprang SR, Gilman AG. The A326S mutant of Gialpha1 as an approximation of the receptor-bound state. J Biol Chem 1998; 273: 21752–8.
26 Berghuis AM, Lee E, Raw AS, Gilman AG, Sprang SR. Structure of the GDP-Pi complex of Gly203→Ala gialpha1: a mimic of the ternary product complex of galpha-catalyzed GTP hydrolysis. Structure 1996; 4: 1277–90.
27 Moreira IS. Structural features of the G-protein/GPCR interactions. BBA-Gen Subjects 2014; 1840: 16–33.
28 Marrari Y, Crouthamel M, Irannejad R, Wedegaertner PB. Assembly and trafficking of heterotrimeric G proteins. Biochemistry 2007; 46: 7665–77.
29 Chen CA, Manning DR. Regulation of G proteins by covalent modification. Oncogene 2001; 20: 1643–52.
30 Winn MD, Ballard CC, Cowtan KD, Dodson EJ, Emsley P, Evans PR, *et al.* Overview of the CCP4 suite and current developments. Acta Crystallogr D 2011; 67: 235–42.
31 Adams PD, Afonine PV, Bunkoczi G, Chen VB, Davis IW, Echols N, *et al.* PHENIX: a comprehensive Python-based system for macromolecular structure solution. Acta Crystallogr D 2010; 66: 213–21.

32 Emsley P, Lohkamp B, Scott WG, Cowtan K. Features and development of Coot. Acta Crystallogr D 2010; 66: 486–501.
33 Karow AR, Gotzl J, Garidel P. Resolving power of dynamic light scattering for protein and polystyrene nanoparticles. Pharm Dev Technol 2015; 20: 84–9.
34 Sasi NK, Tiwari K, Soon FF, Bonte D, Wang T, Melcher K, *et al.* The potent Cdc7-Dbf4 (DDK) kinase inhibitor XL413 has limited activity in many cancer cell lines and discovery of potential new DDK inhibitor scaffolds. PLoS One 2014; 9: e113300.
35 Dickson BM. mu-tempered metadynamics: Artifact independent convergence times for wide hills. J Chem Phys 2015; 143: 234109.
36 Abraham MJ, Murtola T, Schulz R, Páll S, Smith JC, Hess B, *et al.* GROMACS: High performance molecular simulations through multi-level parallelism from laptops to supercomputers. SoftwareX 2015; 1-2: 19–25.
37 Huang J, MacKerell AD Jr. CHARMM36 all-atom additive protein force field: validation based on comparison to NMR data. J Comput Chem 2013; 34: 2135–45.
38 Zoete V, Cuendet MA, Grosdidier A, Michielin O. SwissParam: a fast force field generation tool for small organic molecules. J Comput Chem 2011; 32: 2359–68.
39 Dror RO, Mildorf TJ, Hilger D, Manglik A, Borhani DW, Arlow DH, *et al.* SIGNAL TRANSDUCTION. Structural basis for nucleotide exchange in heterotrimeric G proteins. Science 2015; 348: 1361–5.
40 Laskowski RA, Swindells MB. LigPlot+: multiple ligand-protein interaction diagrams for drug discovery. J Chem Inf Model 2011; 51: 2778–86.
41 Biasini M, Bienert S, Waterhouse A, Arnold K, Studer G, Schmidt T, *et al.* SWISS-MODEL: modelling protein tertiary and quaternary structure using evolutionary information. Nucleic Acids Res 2014; 42 (Web Server issue): W252–8.
42 Lambert NA, Johnston CA, Cappell SD, Kuravi S, Kimple AJ, Willard FS, *et al.* Regulators of G-protein signaling accelerate GPCR signaling kinetics and govern sensitivity solely by accelerating GTPase activity. Proc Natl Acad Sci U S A 2010; 107: 7066–71.
43 Gilchrist A, Vanhauwe JF, Li A, Thomas TO, Voyno-Yasenetskaya T, Hamm HE. G alpha minigenes expressing C-terminal peptides serve as specific inhibitors of thrombin-mediated endothelial activation. J Biol Chem 2001; 276: 25672–9.